Available online at www.sciencedirect.com

ScienceDirect

Proceedings of the Combustion Institute 35 (2015) 215–222

Proceedings of the Combustion Institute

www.elsevier.com/locate/proci

Kinetic studies of the reaction of atomic sulfur with acetylene

Sean Ayling, Yide Gao, Paul Marshall *

Department of Chemistry and Center for Advanced Scientific Computing and Modeling, University of North Texas, 1155 Union Circle #305070, Denton, TX 76203-5017, USA

Available online 25 June 2014

Abstract

The rate constant for reaction of sulfur atoms with acetylene was measured. Laser flash photolysis of CS_2 precursor was employed to generate ground-state $S(^3P)$ atoms, which were monitored with time-resolved resonance fluorescence as they reacted with C_2H_2 in a large excess of Ar bath gas. Temperatures from 295 to 1015 and pressures from 10 to 500 mbar were investigated. A pressure-dependence was observed at all temperatures, revealing that adduct formation is the dominant reaction channel. The necessary stability suggests H_2CCS or possibly HCCSH are the products at high temperatures, so that the reaction is spin-forbidden. The fall-off curves may be represented with a broadening factor $F_{cent} = 0.6$, and low and high-pressure limiting rate constants of $k_0 = 1.0 \times 10^{-18}\,(T/K)^{-3.55}\,\exp(-1990\,K/T)\,cm^6\,molecule^{-2}\,s^{-1}$ and $k_\infty = 2.1 \times 10^{-11}\,\exp(-11.2\,kJ\,mol^{-1}/RT)\,cm^3\,molecule^{-1}\,s^{-1}$, respectively. An entrance barrier to recombination of about 10 kJ mol^{-1} is proposed to arise where the singlet and triplet potential energy curves cross.

Keywords: Acetylene; Sulfur; Kinetics; RRKM theory

1. Introduction

There is a limited amount of data concerning the gas-phase reactivity of C–S bonds. Details of C–S bond breaking or formation are important in a variety of contexts, including astrochemistry, atmospheric chemistry, diamond deposition and the combustion of sulfur-containing fuels. Sulfur–acetylene chemistry has been proposed as part of a mechanism leading to CS_2 formation in the Claus process [1,2]. The presence of sulfur appears to increase the production of PAHs from coal combustion [3] and nanoparticles from diesel combustion [4], and sulfur plays a role in the deposition of diamond-like films with acetylene as the carbon precursor [5]. Organo-sulfur compounds have been detected in comets and the interstellar medium [6,7], where the mechanisms for their formation remain unclear.

Recent computational studies indicate several bound intermediates on the triplet and singlet potential energy surfaces for C_2H_2S which could be collisionally stabilized [8,9]. This would yield pressure-dependent kinetics for the overall reaction

$$S(^3P_J) + C_2H_2(+M) \rightarrow \text{products}(+M) \qquad (1)$$

where M represents a collision partner. However, previous experimental studies of this reaction,

* Corresponding author. Fax: +1 940 565 4318.
E-mail address: marshall@unt.edu (P. Marshall).

http://dx.doi.org/10.1016/j.proci.2014.05.079
1540-7489/

which covered temperatures up to 484 K at fixed pressures of around 300 mbar, did not allow for any pressure dependence for the rate constant k_1 to be revealed [10,11].

Here we present new measurements that span wider ranges of pressure, about 10–500 mbar of Ar, and of temperature, about 300–1000 K. These data reveal that adduct formation is the dominant mechanism and allow some assessment of the thermal stability of these adduct(s). Further, we find that reaction 1 is spin-forbidden and are able to use the pressure dependence of k_1 to investigate the role of intersystem crossing quantitatively, and to compare the low-pressure limit with an RRKM analysis.

2. Methodology

The reagents used were CS_2 (99%, Sigma Aldrich), degassed by freeze–pump-thaw cycles at 77 K, Ar (99.9999%, Air Liquide), used directly, and C_2H_2, degassed and then purified by distillation at 182 K (liquid nitrogen/heptane slush). Gas mixtures were prepared manometrically and stored in glass bulbs.

Sulfur atoms were generated by laser flash photolysis of CS_2 precursor at 193 nm, and monitored by time-resolved resonance fluorescence at 181 nm (^3S–^3P (4s–3p)). Experiments were conducted with a large excess of Ar as a bath gas which served several purposes. It rapidly quenched any excited S(^1D) formed photolytically, it slowed diffusion of S atoms to the reactor walls, it maintained isothermal conditions in the reaction cell and it served as the collision partner M in reaction 1. A general description of the heated reaction cell and details of modifications for S-atom chemistry have been provided previously [12–15]. Briefly, following their pulsed generation, ground-state S(^3P_J) atoms were consumed by reaction with added C_2H_2 or lost by diffusion out of the reaction zone (a volume defined by the intersection of the photolysis and probe beams, each approximately 1 cm across), which was effectively first order. By working under pseudo-first-order conditions with $[C_2H_2] >> [S]$ we may write

$$d[S]/dt = -k_{ps2}[S][C_2H_2] - k_{diff}[S] = -k_{ps1}[S] \quad (2)$$

where k_{ps2} is the effective second-order rate constant for reaction 1 at a given bath gas density [M]. The pseudo-first-order decay coefficient k_{ps1} was obtained from non-linear least squares fits to exponential decays of S-atom resonance fluorescence, which is proportional to [S]. This fluorescence was excited by a microwave-powered discharge lamp through which flowed a dilution of 0.01% H_2S in Ar at ca. 20 Pa pressure. We used Suprasil quartz optics which block H-atom radiation. Fluorescence was detected with a solar blind photomultiplier tube operated in the photon counting mode, and signals from 100–8000 decays were accumulated in a multichannel scaler. An example is shown in Fig. 1. Typically around 4 1/e lifetimes were analyzed. Because this decay is first order, knowledge of absolute [S] is not required. The initial value $[S]_0$ was estimated from $[CS_2]$, its absorption cross section at 193.3 nm, the laser photolysis energy F and the beam cross section of 0.6 cm^2, to ensure that pseudo-first-order condition were attained. Most experiments were carried out with $[S]_0$ of the order of 10^{12} molecule cm^{-3}. At room temperature, where the primary reaction was slowest, higher values up to $\sim 10^{13}$ molecule cm^{-3} were used to verify that secondary chemistry was unimportant. A constant slow flow of reagents ensures each laser pulse encounters a fresh mixture and that products do not accumulate in the reaction zone.

Linear plots of k_{ps1} vs $[C_2H_2]$, such as that shown in Fig. 2, yield the second-order rate constant k_{ps2} as the slope, and its statistical uncertainty. In each experiment $[C_2H_2]$ was varied from zero to a maximum value of the order of 10^{15} molecule cm^{-3}. The small values of F (in the range 0.02–0.1 mJ) and the modest absorption cross section of C_2H_2 at 193.3 nm, $(1.34 \pm 0.05) \times 10^{-19}$ cm^2 $molecule^{-1}$ [16], mean that concentrations of photolytic fragments of C_2H_2 were too small to interfere significantly. The experimental conditions were varied to verify that the observed k_{ps2} were independent of parameters such as F, $[CS_2]$ and $[S]_0$, and the average residence time τ_{res} of gases in the heated reactor before photolysis. This latter variation checks for any thermal decomposition or CS_2–C_2H_2 chemistry, and a dependence was noted at the highest temperatures investigated, $\sim$1015 K. These high-temperature data were therefore plotted as a function of τ_{res} and extrapolated linearly to zero residence time.

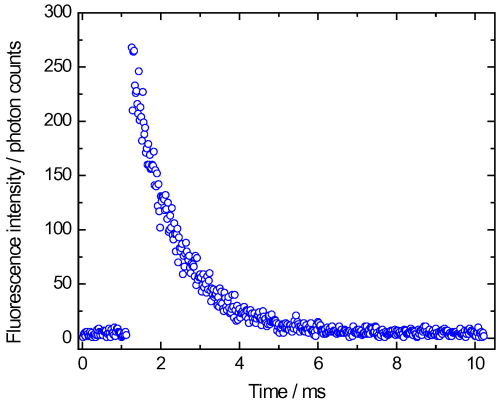

Fig. 1. Example fluorescence signal from S atoms following pulsed photolysis of CS_2 at 1015 K.

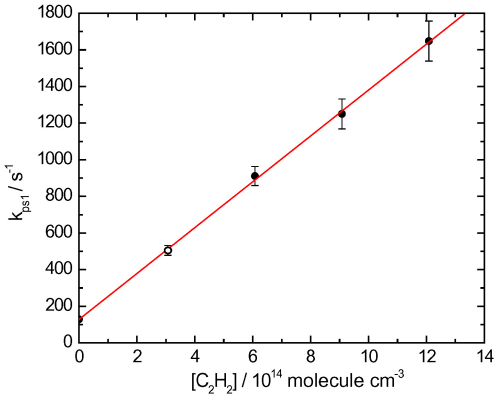

Fig. 2. Plot of k_{ps1} vs acetylene concentration at 1015 K. The open point corresponds to the decay of Fig. 1. Error bars represent $\pm 2\sigma$.

3. Results and discussion

Data from 94 experiments are summarized in Table S1 of the Supplemental material. The k_{ps2} values were found to be independent of the initial radical concentrations, indicating successful isolation of the elementary reaction 1 from secondary processes such as S-atom reaction with the products of the primary reaction 1. There is a clear dependence of k_{ps2} on [Ar], as shown in Fig. 3. This is consistent with a Lindemann–Hinshelwood mechanism of the form

$$S + C_2H_2 \underset{k_{-a}}{\overset{k_a}{\rightleftarrows}} \text{adduct}^* \xrightarrow[+M]{k_b} \text{adduct} \qquad (3)$$

After formation of an initially excited adduct* with rate constant k_a, there is competition between redissociation of the excited adduct (k_{-a}) and stabilization by collision with the bath gas M (k_b). At the limit of low pressure, the collisional stabilization is rate-limiting and $k_{ps2} = k_0$ [M] where k_0 is the third-order low-pressure limit rate constant. At the limit of high pressure all adducts are stabilized, initial addition is rate-limiting, and $k_{ps2} = k_\infty$ which defines the second-order high-pressure limit rate constant. Interpolation between these two regimes is carried out via Troe's formalism [17]

$$k_{ps2} = \left(\frac{k_0[M]}{1 + k_0[M]/k_\infty}\right) \times F_{cent}^{\left\{1+[\log_{10}(k_0[M]/k_\infty)/(0.75-1.27\log_{10}F_{cent})]^2\right\}^{-1}} \qquad (4)$$

The fits are shown in Fig. 3 and the results for the limiting values in Table 1. The scatter on Fig. 3 for the rate constants at 298 K seems large in part because of the small range of k_1 accessible close to the high-pressure limit, which occurs at relatively low pressures at low temperatures. A broadening factor $F_{cent} = 0.6$ was selected, as appropriate for atom + linear reactant [18]. The listed uncertainties of the low-pressure limit and the extrapolated high-pressure limit in Table 1 are purely statistical and are based on the covariance matrix for the sensitivity of the fit to the parameters. We comment that the uncertainty in k_∞ is particularly large at 1015 K because the reaction is not far from the low-pressure limit at the highest temperature and the minor fall-off is weakly sensitive to k_∞.

The nature of the adduct is explored with reference to the computational studies of Woon and Leonori et al. [8,9], who investigated the triplet and singlet surfaces using coupled cluster theory and W1 theory, respectively. We have plotted their results on the same axes in Fig. 4. This potential energy diagram shows that bimolecular products are too endothermic to play a role here, but that candidate adducts are triplet ^{3}CHCHS and singlet c-CHCHS, c-SCCH$_2$, H$_2$CCS and HCCSH. Drawings of these structures are provided in the Supplemental material. The fact that we still observe a pressure dependence at 1015 K indicates that the addition products of reaction 1 must be thermodynamically stable at this temperature. Further, the decays of S atoms remain exponential down to the baseline, with no evidence of a back reaction. This situation can be contrasted to the analogous reaction of O atoms with C_2H_2, where bimolecular products such as CO + CH$_2$ and H + HCCO are favored. We consider the equilibrium

$$S + C_2H_2 \rightleftharpoons \text{adduct} \qquad (5)$$

The concentration equilibrium constant K_c equals [adduct]/([S][C_2H_2]). We define stability here as sufficient to act as a sink for at least half the initial S atoms, and with $[S]_0 << [C_2H_2]$, this implies $K_c > 1/[C_2H_2]$. We evaluate this limit using the median [C_2H_2] in our experiments, and evaluate K_c for the different possible adducts from the partition functions Q and the dissociation enthalpy ΔH_0, using the input data in Table S2 of the Supplementary material:

$$K_c = \frac{Q(\text{adduct})}{Q(S)Q(C_2H_2)} \exp\left(\frac{\Delta H_0}{RT}\right) \qquad (6)$$

The results are compared in Fig. 5. It may be seen that the triplet adduct is insufficiently stable to account for adduct formation even at room temperature, while only H$_2$CCS (ethenethione, the sulfur analog of ketene) and possibly HCCSH (ethynethiol) are stable enough to yield adducts long-lived under our conditions at ~1015 K. Reaction 1 is therefore spin-forbidden.

We now test whether assignment of H$_2$CCS as the dominant product is consistent with our observations via Rice–Ramsperger–Kassel–Marcus (RRKM) theory. The probability of intersystem crossing (ISC) between triplet and singlet surfaces factors equally into the formation and

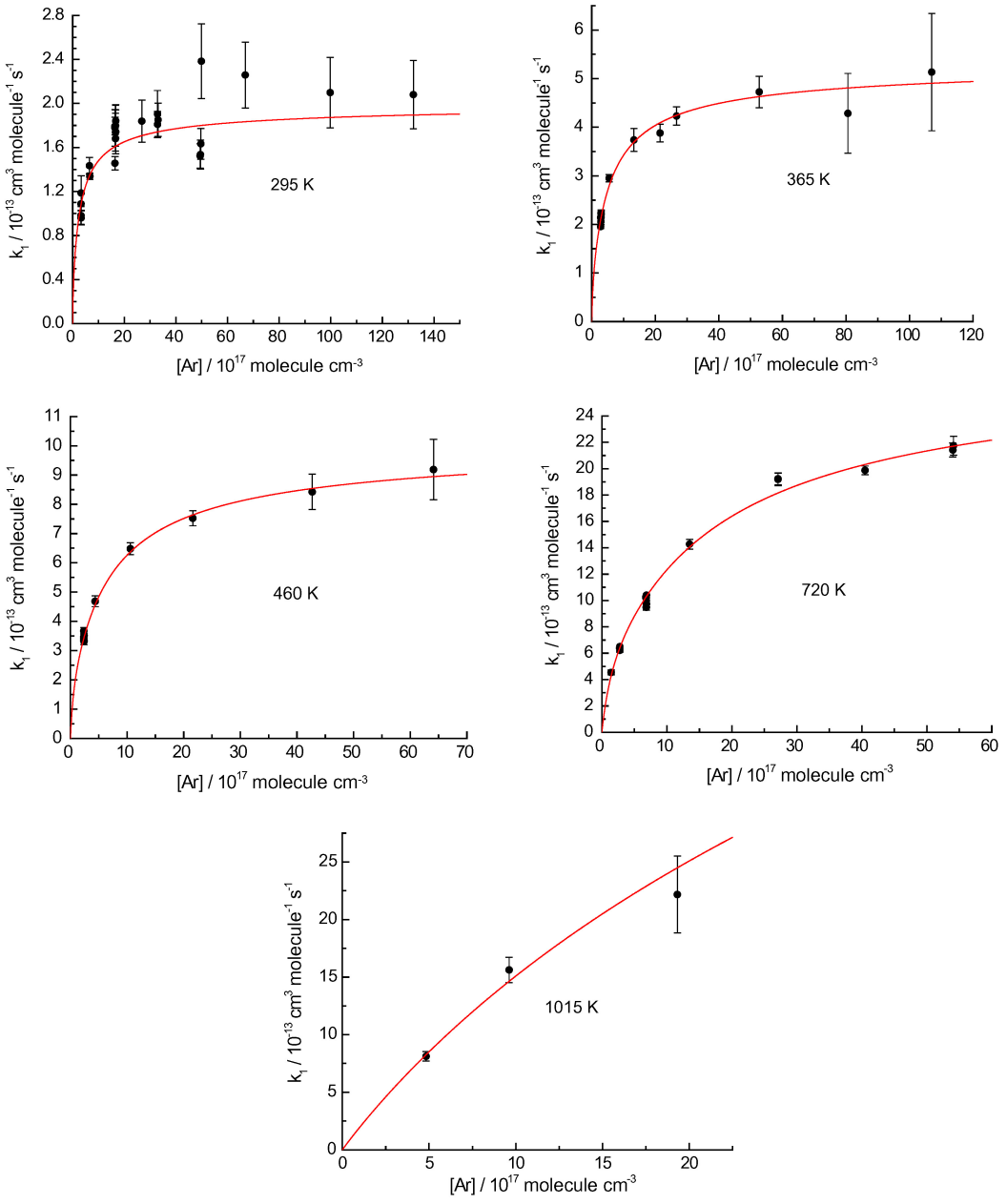

Fig. 3. Pressure dependence of the effective second-order rate constant (error bars $\pm 2\sigma$) for $S + C_2H_2$. Troe fits with $F_{cent} = 0.6$ are superimposed.

dissociation paths in Eq. (3). Because these paths create a pre-equilibrium at the low-pressure limit, this probability does not influence k_0. We set the threshold energy E_0 for dissociation of H_2CCS to $S(^3P) + C_2H_2$ equal to ΔH_0 for dissociation, 304 kJ mol^{-1} computed by Leonori et al. [9], plus 10 kJ mol^{-1} to reflect a barrier E_b observed at the high-pressure limit for recombination (see below). We assume the reaction rate to be negligible below this energy threshold and employ Troe's unimolecular formalism [17] for the dissociation of the adduct:

$$k_{0,diss}/\beta_c = Z_{LJ}\frac{\rho_{vib}(E_0)\,RT}{Q_{vib}(H_2CCS)}F_E F_{anh} F_{rot} \times \exp\left(-\frac{E_0}{RT}\right) \quad (7)$$

Table 1
Results of Troe fitting of $S + C_2H_2$ measurements with F_{cent} fixed at 0.6.

Temperature/K	Low-pressure limit rate constant[a] $k_0/10^{-30}$ cm^6 molecule^{-2} s^{-1}	Collision efficiency β_c	High-pressure limit rate constant[a] $k_\infty/10^{-13}$ cm^3 molecule^{-1} s^{-1}
296	2.09 ± 0.42	0.101	2.13 ± 0.16
366	3.07 ± 0.49	0.089	5.68 ± 0.66
459	4.98 ± 0.53	0.105	11.0 ± 1.0
720	5.49 ± 0.43	0.110	31.4 ± 2.1
1013	2.47 ± 0.58	0.074	141 ± 63

[a] Statistical uncertainty is 2σ.

Because K_c (Eq. (6)) is the ratio of addition to dissociation rate constants $k_{0,add}/k_{0,diss}$, and $E_0 - \Delta H_0 = E_b$, we may write

$$k_{0,add}/\beta_c = Z_{LJ}\frac{\rho_{vib}(E_0)\,RT}{Q_{vib}(H_2CCS)} \times \frac{Q(H_2CCS)}{Q(S)Q(C_2H_2)} F_E F_{anh} F_{rot} \times \exp\left(-\frac{E_b}{RT}\right) \quad (8)$$

where the symbols have their usual meanings. β_c represents the collisional efficiency of the Ar bath gas. Z_{LJ} is the Lennard–Jones rate constant, based on σ and ε/k_BT parameters for Ar and H_2CCS of 3.47 Å and 114 K, and 4.35 Å and 300 K, respectively (the latter values are a guess, based on values for C_2H_2 and H_2S. Z_{LJ} is not very sensitive to the particular numbers.) Q is the partition function, ρ is the density of states, and the F terms are corrections for the energy dependence of the density of states, vibrational anharmonicity and angular momentum effects. The ratio of the two largest moments of inertia at the geometry at the crossing point relative to those of H_2CCS yield $I^+/I = 1.05$ which contributes to F_{rot}. β_c was initially chosen to fit Eq. (8) to the experimental k_0 points and is listed in Table 1. The associated average energy transferred per collision with Ar was found to be approximately represented as $-\langle\Delta E\rangle_{all} = 400$ (T/298 K) J mol^{-1} which is within typical values for other reactions [19]. The corresponding temperature dependence of k_0 can be summarized as $k_0 = 1.0 \times 10^{-18}$ (T/K)$^{-3.55}$ exp(−1990 K/T) cm^6 molecule^{-2} s^{-1} and is compared to experiment on Fig. 6. At moderate temperatures the recombination rate constant increases with temperature because of the barrier to be overcome, while at high temperatures the most important factor is the decrease in collisional efficiency with increasing temperature. Similar behavior was seen in the spin-forbidden addition of O atoms to SO_2 [20].

The high-pressure limit for reaction 1 is plotted in Arrhenius form in Fig. 7, and a weighted fit can be expressed as

$$k_\infty = (2.1 \pm 0.7) \times 10^{-11} \exp(-11.2 \pm 1.2 \text{ kJ mol}^{-1}/RT) \text{cm}^3\text{molecule}^{-1}\text{ s}^{-1} \quad (9)$$

where the uncertainties are $\pm 2\sigma$ in the Arrhenius parameters. The earlier measurements [10,11] should correspond to this high-pressure limit and are also plotted there. They lie a factor of ca. 2 larger than the present results, which might reflect an influence of secondary chemistry in the prior work. k_∞ corresponds to the rate constant for formation of initially excited adducts in the scheme shown in Eq. (3) and is proportional to the probability of ISC. The rate constant is $\sim 4 \times 10^{-10}$ cm^3 molecule^{-1} s^{-1} for the spin-allowed addition of singlet S(^{1}D) to acetylene [9], which tells us the collision rate between S atoms and C_2H_2, so we may estimate the ISC probability for S(^{3}P) addition per collision as ca. 5%. This probability is in the range of values proposed for other spin-forbidden addition reactions of S(^{3}P), such as ~1% for $S + CS_2$ [21] and ~20% for $S + H_2S$ [22].

The temperature dependence in Eq. (7) suggests the presence of an energy barrier to S(^{3}P) addition, so we have explored some of the geometries where ISC may occur. We used B3LYP/6-311G(2d,d,p) density functional theory implemented with the Gaussian 09 program [23] to evaluate singlet energies as S was brought towards C_2H_2 from the side, in a C_{2V} geometry. The other geometry parameters were allowed to relax as a function of r, the distance between S and the center of C_2H_2. The singlet and triplet energies were calculated at these same geometries using the CBS-QB3 method (excluding zero-point vibrational energy) [24], and the results are plotted as a function of r in Fig. 8. As expected from prior work where there is no barrier to formation of thiirene [9] and the triplet analog is significantly endothermic [8], the long-range singlet potential is attractive while the triplet potential is repulsive, so there is a crossing, which we locate at $r = 2.47 \times 10^{-10}$ m. The energy here (excluding zero point energy) is 11.4 kJ mol^{-1} above the ground state reactants, which becomes 9.7 kJ mol^{-1} after correction for zero-point energy changes. This is

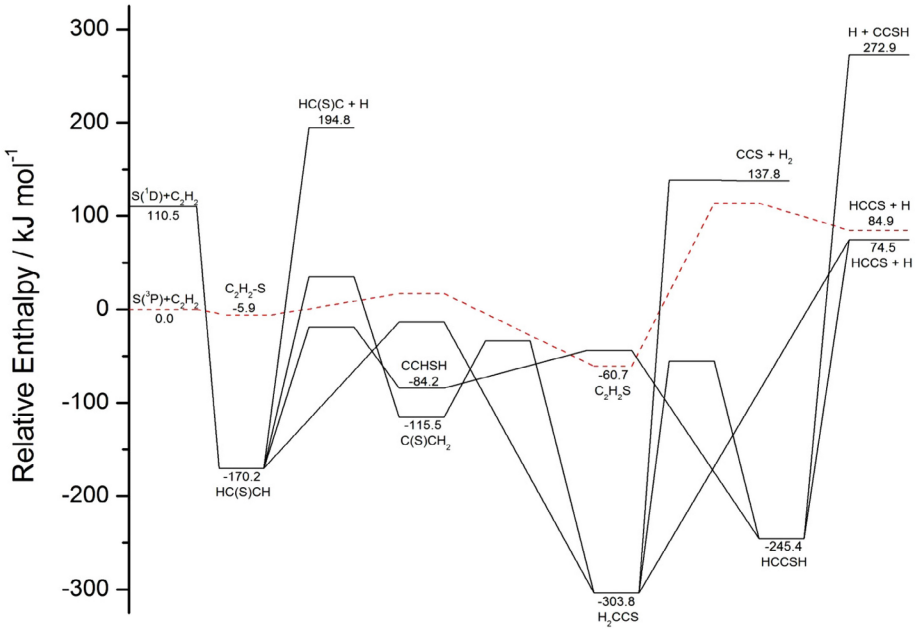

Fig. 4. Potential energy diagram for $S + C_2H_2$ showing triplet species (dashed line, Woon; Ref. [8]) and singlet species (solid line, Leonori et al.; Ref. [9]). Enthalpies are relative to $S(^3P) + C_2H_2$ at 0 K.

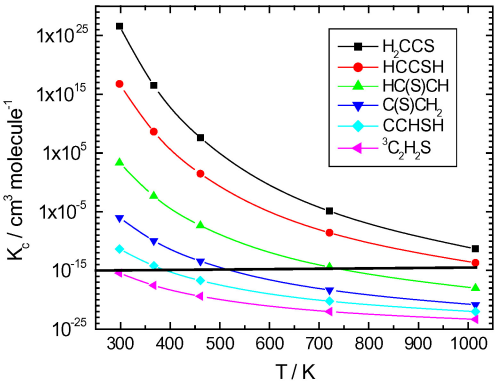

Fig. 5. Computed equilibrium constant K_c for $S + C_2H_2 \rightleftharpoons$ adduct for a variety of candidates. The line is the approximate minimum value of K_c necessary for adduct formation to dominate experimentally.

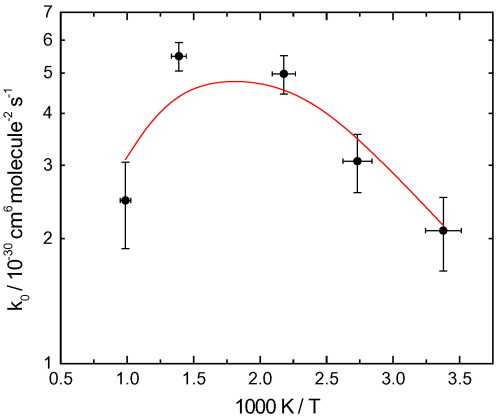

Fig. 6. Low-pressure limit rate constants k_0 for $S + C_2H_2$. The points are measurements with $\pm 2\sigma$ error bars. The line is from the Troe unimolecular formalism (see text).

fortuitously close to the observed activation energy in Eq. (9). These are not formally identical quantities but the accord suggests the temperature dependence can be rationalized in terms of an ISC-induced barrier. This analysis does not rule out the existence of other ISC regions elsewhere on the PES. For example, in the analogous reaction of triplet O atoms with C_2H_2, exothermic fragmentation rather than stabilization is observed, with the major products being $H + HCCO$ and $CO + CH_2$ in triplet and singlet states. Formation of $^1CH_2$ is spin-forbidden and a recent analysis [25] suggests the overall fraction of collisions leading to $CO + {}^1CH_2$ is $7 \pm 3\%$, which is higher than might be expected given the weak spin–orbit coupling of oxygen. Unlike reaction 1, there is a strongly bound, long-lived triplet HCCHO adduct which allows for multiple trajectories to explore an ISC region leading to ketene.

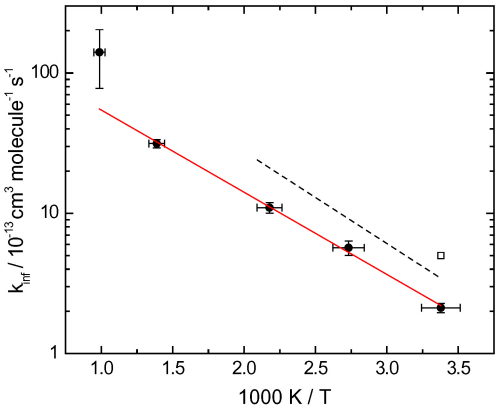

Fig. 7. Arrhenius plot of high-pressure limit rate constants k_∞ for $S + C_2H_2$. The filled points are present measurements with $\pm 2\sigma$ error bars in temperature and rate constant. The open symbol and dashed line are the results from Refs. [10,11].

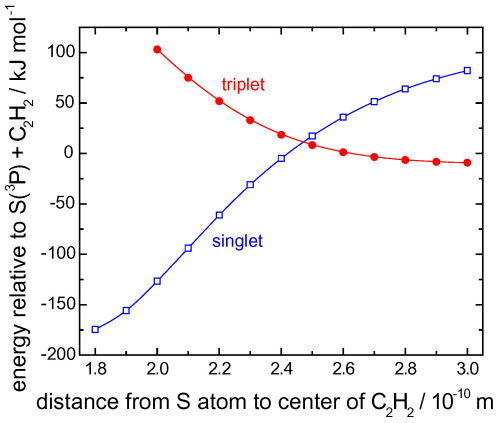

Fig. 8. Singlet (open squares) and triplet (solid circles) energies for sideways approach of S to C_2H_2 calculated at the CBS-QB3 level of theory.

Another difference from reaction 1 is that formation of spin-allowed $CS + {}^3CH_2$ is endothermic by 161 kJ mol^{-1} [26].

4. Conclusions

New pressure-dependent measurements show that adduct formation is the dominant mechanism even at the highest temperatures explored, ~1015 K. A combination of potential energy information from the literature with the necessary thermal stability to account for the observations suggests H_2CCS is the likely candidate at the highest temperatures, although HCCSH might also play a role. The reaction is spin-forbidden and the high-pressure limit can be rationalized in terms of a 5% probability for intersystem crossing and a ca. 10 kJ mol^{-1} barrier to recombination, which is consistent with our initial exploration of triplet-singlet curve crossing. The low-pressure limit is rationalized via RRKM theory and reasonable energy transfer parameters.

Acknowledgments

We thank the Robert A. Welch Foundation (Grant B-1174) and the National Science Foundation (Grant CBET-0756144) for support. Computational facilities were purchased with NSF Grant CHE-0741936.

Appendix A. Supplementary data

Supplementary data associated with this article can be found, in the online version, at http://dx.doi.org/10.1016/j.proci.2014.05.079.

References

[1] W.D. McGrath, T. Morrow, D.N. Dempster, *Chem. Commun.* (1967) 516–518.
[2] I.A. Gargurevich, *Ind. Eng. Chem. Res.* 44 (2005) 7706–7729.
[3] K. Liu, W. Han, W.-P. Pan, J.T. Riley, *J. Hazard. Mater.* B84 (2001) 175–188.
[4] Z.D. Ristovski, E.R. Jayaratne, M. Lim, G.A. Ayoko, L. Morawska, *Environ. Sci. Technol.* 40 (2006) 1314–1320.
[5] R. Haubner, D. Sommer, *Diamond Relat. Mater.* 12 (2003) 298–305.
[6] N. Dello Russo, M.A. DiSanti, M.J. Mumma, K. Magee-Sauer, T.W. Rettig, *Icarus* 135 (1998) 377–388.
[7] J. Benkhoff, D.C. Boice, *Planet. Space Sci.* 44 (1996) 665–673.
[8] D.E. Woon, *J. Phys. Chem. A* 111 (2007) 11249–11253.
[9] F. Leonori, R. Petrucci, N. Balucani, K.M. Hickson, M. Hamberg, W.D. Geppert, P. Casavecchia, M. Rosi, *J. Phys. Chem. A* 113 (2009) 4330–4339.
[10] D.J. Little, R.J. Donovan, *J. Photochem.* 1 (1973) 371–377.
[11] A. van Roodselaar, I. Safarik, O.P. Strausz, H.E. Gunning, *J. Am. Chem. Soc.* 100 (1978) 4068–4073.
[12] Y. Shi, P. Marshall, *J. Phys. Chem.* 95 (1991) 1654–1658.
[13] L. Ding, P. Marshall, *J. Phys. Chem.* 96 (1992) 2197–2201.
[14] L. Ding, P. Marshall, *J. Chem. Soc., Faraday Trans.* 89 (1993) 419–423.
[15] A. Goumri, D.D. Shao, P. Marshall, *J. Chem. Phys.* 121 (2004) 9999–10005.
[16] K. Seki, H. Okabe, *J. Phys. Chem.* 97 (1993) 5284–5290.
[17] J. Troe, *J. Phys. Chem.* 83 (1979) 114–126.
[18] C.J. Cobos, J. Troe, *Z. Phys. Chem.* 217 (2003) 1031–1044.

[19] H. Endo, K. Glänzer, J. Troe, *J. Phys. Chem.* 83 (1979) 2083–2090.
[20] J. Naidoo, A. Goumri, P. Marshall, *Proc. Combust. Inst.* 30 (2005) 1219–1225.
[21] Y. Gao, P. Marshall, *J. Chem. Phys.* 135 (144306) (2011) 1–12.
[22] Y. Gao, C. Zhou, K. Sendt, B.S. Haynes, P. Marshall, *Proc. Combust. Inst.* 33 (2010) 459–465.
[23] M.J. Frisch et al., *Gaussian 09*, Gaussian, Wallingford, CT, 2009.
[24] J.A. Montgomery Jr., M.J. Frisch, J.W. Ochterski, G.A. Petersson, *J. Chem. Phys.* 110 (1999) 2822–2827.
[25] K. Rajak, B. Maiti, *J. Chem. Phys.* 133 (011101) (2010) 1–4.
[26] NIST Computational Chemistry Comparison and Benchmark Database, NIST Standard Reference Database Number 101, Release 16a, August 2013, Ed: R.D. Johnson III (http://cccbdb.nist.gov).